Upconversion superburst with sub-2 μs lifetime

Yiming Wu, Jiahui Xu, Eng Tuan Poh, Liangliang Liang, Hailong Liu, Joel Yang, Cheng-Wei Qiu, Renaud Vallée, Xiaogang Liu

Upconversion superburst with sub-2 μs lifetime

Yiming Wu[1†], Jiahui Xu[1†], Eng Tuan Poh[2], Liangliang Liang[1], Hailong Liu[3], Joel K.W. Yang[3], Cheng-Wei Qiu[4], Renaud A. L. Vallée[5]* & Xiaogang Liu[1,6,7]*

[1]Department of Chemistry, National University of Singapore, Singapore 117543, Singapore. [2]Graduate School for Integrative Science and Engineering (NGS), National University of Singapore, Singapore 117456, Singapore. [3]Singapore University of Technology and Design, Singapore 487372, Singapore. [4]Department of Electrical and Computer Engineering, National University of Singapore, Singapore 117583, Singapore. [5]CNRS, University of Bordeaux, CRPP-UMR 5031, Pessac 33600, France. [6]The N.1 Institute for Health, National University of Singapore, Singapore 117456. [7]Joint School of National University of Singapore and Tianjin University, International Campus of Tianjin University, Fuzhou, 350207, P. R. China.

[†]These authors contributed equally.

Corresponding authors. E-mail: chmlx@nus.edu.sg; renaud.vallee@u-bordeaux.fr

The generation of anti-Stokes emission through lanthanide-doped upconversion nanoparticles is of great importance for technological applications in energy harvesting, bioimaging, and optical cryptography[1-3]. However, the weak absorption and long radiative lifetimes of upconversion nanoparticles may significantly limit their use in imaging and labeling applications in which a fast spontaneous emission rate is essential[4-6]. Here, we report the direct observation of upconversion superburst with directional, fast and ultrabright luminescence by coupling gap plasmon modes to nanoparticle emitters. Through precise control over the nanoparticle's local density of state, we achieve emission amplification by 4-5 orders of magnitude and a 166-fold rate increase in spontaneous emission. We also demonstrate that tailoring the mode of the plasmonic cavity permits active control over the color output of upconversion emission. These findings may benefit the future development of rapid nonlinear image scanning nanoscopy and open up the possibility of constructing high-frequency, single-photon emitters driven by telecommunication wavelengths.

Although many luminescent systems such as organic dyes and quantum dots have been explored as the candidates to realize photon upconversion within nanometric volumes through molecular triplet-triplet annihilation[7], second harmonic generation[8] or multiphoton absorption processes[9], lanthanide-doped upconversion nanoparticles (UCNPs) are ideal candidates for nonlinear upconversion of infrared excitation because of their excellent photostability, massive anti-Stokes shift, and exceptional thermal sensitivity[10-12]. Despite the

potential, the current development of UCNPs is hindered by the low quantum yield of energy conversion and slow spontaneous emission rates. Given the fact that radiative transitions in the inner 4f shell of lanthanide ions are parity forbidden[13-16], UCNPs generally exhibit weak and narrowband absorption and long radiative lifetimes on the order of hundreds of microseconds to milliseconds. Early experiments have shown that plasmonic structures can provide locally enhanced electromagnetic fields to amplify the upconversion process within sub-diffraction volumes[17, 18]. However, the maximum enhancement reported so far in the spontaneous emission rate for UCNPs through plasmonic coupling has been limited to a factor of 8, which creates a large gap between theory and its application to practical problems[19].

Our idea to achieve fast upconversion emission consists of coupling the emission of UCNPs to gap-mode plasmonic nano-resonators (Fig. 1a, b). We reason that the rate of spontaneous upconversion emission could be boosted by manipulating the nanoparticle's local density of state through Purcell effects. According to Fermi's golden rule, the spontaneous emission rate (γ_{sp}) of an emitter that is not in free space is proportional to the local density of optical states[20, 21]:

$$\gamma_{sp}(r) = \frac{\pi\omega}{3\hbar\epsilon_0}|p|^2\rho(r,\omega) \qquad (1)$$

where ω is the emission frequency, p is the transition dipole moment of the emitter, r is the position, ϵ_0 is the permittivity of free space and $\rho(r,\omega)$ is the electromagnetic local density of states at frequency ω. In a dedicated resonant cavity, the local density of states can be greatly increased, and the spontaneous emission rate of an embedded emitter can be enhanced by the Purcell factor[22, 23]

$$F = \frac{\gamma_{sp}}{\gamma_0} = \frac{3}{4\pi^2}\left(\frac{Q}{V_{mode}}\right)\left(\frac{\lambda}{n}\right)^3 \qquad (2)$$

where Q is the cavity quality factor, V_{mode} is the mode volume, λ is the resonant wavelength, n is the refractive index of the medium and γ_0 is the spontaneous emission rate of the emitter in free space. This formula indicates that a significant increase in the emission rate requires an optical resonator that can spatially confine the light field in a small mode volume for an extended period. Thus, while possessing a modest cavity quality factor, a plasmonic nanocavity could still exhibit a large Purcell factor due to the nanoscopic mode volume[24, 25]. UCNPs in the plasmonic nanocavity are likely to experience a substantial acceleration of their spontaneous emission and exhibit significant luminescence enhancement.

To validate our hypothesis, we designed a plasmonic cavity consisting of a silver nanocube-coupled gold mirror structure with a nanoscale gap filled with UCNPs (Fig. 1b, c). We next performed three-dimensional finite-difference-time-domain (3D-FDTD) simulations (Supplementary Fig. 1) to guide the structural design of the cavity and ensure an optimal matching between the known UCNPs and the cavity mode, both spectrally and spatially. As depicted in Figure 1d-f, the designed individual nanocavity with a gap thickness of 20 nm and Ag nanocube ~90 nm in edge length exhibits a plasmon resonance mode of $\lambda \approx 660$ nm, spectrally overlapping with the emission of Er^{3+}-activated UCNPs, and possesses the maximum radiative decay rate at the wavelength of 660 nm. Our simulation results also revealed that the fundamental plasmonic mode of the film-coupled nanocube is localized in the gap with a maximum field enhancement ($|E/E_0|$) up to 40 (Fig. 1c; Supplementary Fig. 2). Apart from confining the radiative emission field into a nanometric photonic hotspot of extremely high field intensity, the plasmonic nanocavity can also enhance the extraction efficiency of far-field light[20]. Through 3D-FDTD simulations, the far-field radiation pattern of the plasmonic nanocavity at the resonance wavelength is found to have a single lobe normal to the surface (Fig. 2a, b; Supplementary Figs. 3 and 4), which is ideal for light collection and coupling to external optics[26]. For example, when using an objective lens with a numerical aperture of 0.9, the calculated collection efficiency for the emitted light remains very large (~85%), which is approximately 4.5-fold higher than that of the control sample directly placed on a glass slide (Fig. 2b, c; Supplementary Figs. 3-5). Such highly directional emission and high collection efficiency are particularly suited to light extraction from the cavity in favor of emission amplification.

To exploit the possibility of coupling UCNPs to the gap-mode nanocavity for maximum emission enhancement, we investigated the excited-state absorption (ESA)-mediated upconversion process in the plasmonic nanocavity (Supplementary Fig. 6). Figure 2d presents both the ESA enhancement factor arising from the fourth power of the near-field enhancement and the relaxation factor due to the spontaneous transition from an intermediate state to the ground state as a function of depth of the emitter within the gap. When the upconversion emission is resonant with the plasmon mode, the nanocavity exhibits a dramatic enhancement in the spontaneous emission rate (γ_{sp}) relative to the emission rate in free space (γ_0). The calculated emission rate depends on the lateral position of the emitter under the nanocube, with maximum rate enhancements exceeding 700 near the corners of the nanocube (Fig. 2e). At the same time, the maximum radiative quantum yield enhancement (η/η_0) is predicted to increase by a factor of ~ 600 (Fig. 2f).

These theoretical results suggest that gap-mode plasmonic nanocavity provides an excellent platform to boost spontaneous emission rate and significantly improve the upconversion efficiency.

We further experimentally investigated the feasibility of our design to accelerate the nonlinear upconversion process. In our study, $NaYF_4$:Yb/Er (18/2 mol %) nanoparticles of ~20 nm in diameter were selected and synthesized (Supplementary Fig. 7) for their known efficient upconversion process[11, 27]. We also synthesized Ag nanocubes with well-controlled sizes for the construction of the plasmonic nanocavity (Supplementary Fig. 8)[28]. The UCNPs/plasmonic nanocavity hybrid system was realized through bottom-up assembly (Supplementary Fig. 9). Individual UCNP/plasmonic nanocavities were identified by dark-field and fluorescence imaging, followed by spectroscopic measurement on the located nanoparticles. Under excitation at 980 nm, Er^{3+}-activated UCNPs showed two characteristic emissions at 554 and 660 nm (Supplementary Fig. 6).

Figure 2g shows luminescence imaging of a monolayer of UCNPs self-assembled on a gold substrate with a partial Ag nanocube coverage. When the Ag nanocubes were present on the top of UCNPs to form gap-mode nanocavities, such UCNPs showed a bright yellow-red emission, while only inconspicuous luminescence was captured in the absence of the Ag nanocubes. The same region was subsequently imaged with a scanning electron microscope (SEM) to examine the size and shape of the gap-mode nanocavity under study (Fig. 2h, i). It is important to note that when the size of the Ag nanocube decreased, selective enhancement of green emission was observed (Supplementary Fig. 10), indicating a possible control over the radiative emission process of UCNPs using size-tunable Ag nanocubes. The fundamental mode of a single resonant nanocavity was also verified by dark-field scattering spectroscopy (Fig. 3a). The simulated scattering spectrum of a single plasmonic nanocavity exhibited a maximum resonance peak around 660 nm with a narrow bandwidth, while the measured scattering spectrum showed a similar resonance wavelength near 660 nm. The resonance broadening of the measured spectrum could be attributed to the inhomogeneous dielectric environment in the plasmonic cavity.

To gain more insight into the Purcell-enhanced upconversion process and quantify the luminescence enhancement, we performed a series of optical characterizations. These include measurements on a sample containing plasmonic cavity-coupled UCNPs and two control samples, with one sample adhered on a gold film without the coverage of Ag nanocubes and the other directly deposited onto a glass slide. Luminescence spectra measurements of UCNPs within the plasmonic nanocavities were first carried out using our custom-built microscope. The 980 nm continuous wave excitation laser was coupled to the

optical microscope and focused to an excitation spot of 15 μm diameter, and 64 isolated nanocavities were located within this area. The upconversion luminescence was then collected using a fiber-coupled optical spectrometer. Similar optical measurements of the two control samples were also conducted under the same experimental conditions. Figure 3b depicts the typical luminescence spectra of the three different samples at an excitation power of 7.5 mW. The luminescence intensity from UCNPs coupled to plasmonic nanocavities is substantially larger than that of the nanoparticles deposited on either a gold film or a glass slide. For UCNPs directly deposited on the gold film, the luminescence intensity at 660 nm decreased by ~ 50% compared to that of the control sample deposited on a glass substrate, indicative of nonradiative energy transfer between UCNPs and the gold film.

For upconversion nanomaterials, the intensity of their emission *I*, arising from an *n*-photons populated state, increases as a power function of excitation power *P* ($I \propto P^n$) and eventually reaches a plateau[29, 30]. In this work, we carried out the power-dependent investigations of luminescence intensity at 554 and 660 nm for UCNPs coupled to the plasmonic nanocavity and the two control substrates (Supplementary Fig. 11). The double-logarithmic plots of the emission intensity versus pumping power were shown in Figure 3c and d. We found that the slopes (*n*) of green and red emission collected from the glass substrate are 1.15 and 1.38, but change to 1.41 and 1.82 from the gold substrate under weak excitation. This discrepancy could be attributed to the nonradiative energy transfer between UCNPs and the gold film. Contrastedly with the two aforementioned situations, the slopes (*n*) of the green and red emissions collected from the nanocavities were reduced to 0.84 and 1.00 under weak excitation. The diminished slopes could be ascribed to the fact that the introduction of nanocavities creates plasmonic hotspots with high local excitation power. Although the output power of the laser source is not changed, UCNPs embedded in the nanocavities are likely to probe a much higher pumping photon flux to excite Er^{3+} ions from the ground state to the emitting excited state. As a result, the UCNPs coupled to the nanocavities will rapidly reach an upconversion saturation state and give rise to a reduced slope. The average enhancement factor ⟨EF⟩ in luminescence intensity from the cavity-coupled UCNPs relative to that on glass and gold film was further quantified and calculated according to

$$\langle EF \rangle = \frac{I_{cavity} - I_{gold}}{I_{glass/gold}} \times \frac{A_{spot}}{A_{cavity}} \qquad (3)$$

where I_{cavity} is the emission intensity from the sample containing 64 individual plasmonic nanocavities under 15 μm diameter excitation spot, I_{gold} and I_{glass} are the emission intensity from UCNPs deposited either on the gold film or glass control samples under the same laser excitation spot. A_{spot} is the area of the excitation spot and A_{cavity} is the area under the nanocube. The area under the nanocube is given by $A_{cavity} = NL^2$ where *N* is the numbers of Ag nanocube and *L* is the side length of Ag nanocube without the ligand layer. The power-dependent investigations of emission enhancement factor revealed that the effect of pump fluence on emission intensity is more predominant under low power than under high power excitation. We found that the intensity of red emission is enhanced by a factor of ~1.01 × 10^4 and ~1.8 × 10^3 at low and high pumping power, respectively, while the green emission is intensified by a factor of ~1.6 × 10^3 and ~1.9 × 10^2 at low and high pumping power, respectively (Fig. 3e). In addition, a luminescence enhancement factor of up to 3.3 ×10^4 was obtained for UCNPs coupled to the nanocavity relative to the gold film (Fig. 3f).

The total emission enhancement of photon upconversion originates from three processes: an enhanced light extraction α, an enhanced excitation rate β, and the quantum efficiency enhancement originating from the Purcell effect (see Methods), resulting in an average luminescence enhancement factor:

$$\langle EF \rangle = \alpha\beta\,\eta(\omega)/\eta_0(\omega) \qquad (4)$$

Together with the abovementioned numerical analyses, we estimated the enhancement factor ⟨EF⟩ relative to dipoles deposited on a bare glass substrate to be ~ 7000 for gap plasmon mode-coupled UCNPs. The theoretical discrepancy in the enhancement factor may be attributed in part to the lack of full consideration of the complex energy transfer processes in the ESA-mediated theoretical model. The discrepancy may also arise from the broadening of the measured scattering spectrum, due to the inhomogeneous dielectric environment in the plasmonic gap, which was not considered in simulations. Both factors could amount to a significant increase in the excitation flux, as evidenced by the reduced population time due to increased population kinetics for the $^2F_{7/2} \rightarrow {}^2F_{5/2}$ transition of Yb^{3+} ion (Fig. 4a, b; Supplementary Fig. 12).

We next measured and compared the decay dynamics of excited UCNPs, either placed on a glass slide or a gold film or within the plasmonic nanocavity, by time-resolved spectroscopy. The normalized transient kinetic traces were recorded for both emission wavelengths at 554 and 660 nm. The UCNPs on the glass slide showed monoexponential decay with slow decay lifetimes of 143 and 232 μs at 554 and 660 nm, respectively (Fig. 4a,

c; Supplementary Fig. 12). Compared with UCNPs deposited on the glass slide, UCNPs adhered to the gold film showed slightly shortened lifetimes of 100 and 180 μs at 554 and 660 nm (Supplementary Fig. 12), respectively, but with reduced intensity as a result of nonradiative quenching effects of gold films (Fig. 3b). In contrast, the UCNPs in the plasmonic nanocavity showed a dramatically shortened luminescence lifetime, accompanied by a significant increase in emission intensity. Since the measured luminescence is a summation of the emissions from UCNPs coupled to the gap-mode nanocavity and neighboring UCNPs without the coupling, the transient decay kinetics are expected to fit into the sum of two exponential decay components:

$$I(t) \approx Aexp\left(-t/\tau_{coupled}\right) + Bexp\left(-t/\tau_{uncoupled}\right) \qquad (5)$$

where *I* is the luminescence intensity, *t* is the decay time, *A* and *B* are the double-exponential fitted amplitudes for fast and slow decay components, and $\tau_{coupled}$ and $\tau_{uncoupled}$ are the fast and slow time constants.

We recorded a slow decay component of 157 μs ($\tau_{cavity}^{660,s}$) for uncoupled UCNPs and a fast decay component of 1.4 μs ($\tau_{cavity}^{660,f}$) for UCNPs coupled to the nanocavity, indicating a 166-fold decay rate enhancement (Fig. 4d). On the other hand, a decay rate enhancement of 23.8 was observed for green emission at 554 nm (Fig. 4b). Such a substantial enhancement of decay rate is 20 times more than the largest value reported for an UCNP-3D plasmonic nanostructure[19]. It should also be noted that because of our detector's resolution limit, the measured value of the cavity-coupled UCNPs provides only an upper bound on the lifetime.

We have theoretically and experimentally demonstrated that gap plasmon modes could be used to mitigate the fundamental constraints of parity-forbidden 4f-4f transitions in lanthanide-doped nanocrystals, providing an effective way to realize upconversion superburst with fast, ultrabright and highly directional spontaneous emission. The strong nanocavity-UCNP coupling is capable of achieving a more than 10,000-fold enhancement of spontaneous emission and a rate increase 166 times faster than those control samples without the nanocavity. Additionally, the colloidally templated nanocavity offers an inherently inexpensive and flexible plasmonic platform, particularly suitable for planar fabrication process and scale-up applications. This platform not only provides a valuable tool in investigating the boundaries of photon-matter interactions but also enables a myriad of potential applications in quantum optics, from solid-state single-photon emitters to low-threshold infrared quantum counters.

Online content

Methods, along with any additional Supplementary display items and Source Data, are available in the online version of the paper; references unique to these sections appear only in the online paper.

References

1. Huang, X., Han, S., Huang, W., & Liu, X. Enhancing solar cell efficiency: the search for luminescent materials as spectral converters. *Chem. Soc. Rev.* **42**, 173-201 (2013).
2. Lu, Y. et al. Tunable lifetime multiplexing using luminescent nanocrystals. *Nat. Photonics* **8**, 32-36 (2014).
3. Chen, S. *et al*. Near-infrared deep brain stimulation via upconversion nanoparticle-mediated optogenetics. *Science* **359**, 679–684 (2018).
4. Chen, X. *et al*. Confining energy migration in upconversion nanoparticles towards deep ultraviolet lasing. *Nat. Commun.* **7**, 10304 (2016).
5. Liu, Y. *et al*. Amplified stimulated emission in upconversion nanoparticles for super-resolution nanoscopy. *Nature* **543**, 229–233 (2017).
6. Fan, Y. *et al*. Lifetime-engineered NIR-II nanoparticles unlock multiplexed in vivo imaging. *Nat. Nanotechnol.* **13**, 941 (2018).
7. Wu, M. *et al*. Solid-state infrared-to-visible upconversion sensitized by colloidal nanocrystals. *Nat. Photonics* **10**, 31–34 (2016).
8. Chen, C. K., De Castro, A. R. B. & Shen, Y. R. Surface-enhanced second-harmonic generation. *Phys. Rev. Lett.* **46**, 145–148 (1981).
9. Chen, W. *et al*. Giant five-photon absorption from multidimensional core-shell halide perovskite colloidal nanocrystals. *Nat. Commun.* **8**, 15198 (2017).
10 Liu, Q. *et al*. Single upconversion nanoparticle imaging at sub-10 W cm^{-2} irradiance. *Nat. Photonics* **12**, 548-553 (2018).
11. Wu, S. *et al*. Non-blinking and photostable upconverted luminescence from single lanthanide-doped nanocrystals. *Proc. Natl. Acad. Sci.* **106**, 10917–10921 (2009).
12. Zhou, B., Shi, B., Jin, D. & Liu, X. Controlling upconversion nanocrystals for emerging applications. *Nat. Nanotechnol.* **10**, 924–936 (2015).
13. Renero-Lecuna, C. *et al*. Origin of the high upconversion green luminescence efficiency in β-$NaYF_4$:2%Er^{3+},20%Yb^{3+}. *Chem. Mate*r. **23**, 3442–3448 (2011).
14. Zhao, J. et al. Single-nanocrystal sensitivity achieved by enhanced upconversion luminescence. *Nat. Nanotechnol*. **8**, 729–734 (2013).
15. Laporte, O. & Meggers, W. F. Some rules of spectral structure. *J. Opt. Soc. Am.* **12**, 459–463 (1925).
16. Malta, O. L. Mechanisms of non-radiative energy transfer involving lanthanide ions revisited. *J. Non. Cryst. Solids* **354**, 4770-4776 (2008).
17. Park, W., Lu, D. & Ahn, S. Plasmon enhancement of luminescence upconversion. *Chem. Soc. Rev.* **44**, 2940-2962 (2015).
18. Das, A., Mao, C., Cho, S., Kim, K., Park, W. Over 1000-fold enhancement of upconversion luminescence using water-dispersible metal-insulator-metal nanostructures. *Nat. Commun.* **9**, 4828 (2018).

19. Zhang, W., Ding, F. & Chou, S. Y. Large enhancement of upconversion luminescence of $NaYF_4:Yb^{3+}/Er^{3+}$ Nanocrystal by 3D plasmonic nano-antennas. *Adv. Mater.* **24**, OP236-OP241 (2012).
20. Akselrod, G. M. et al. Probing the mechanisms of large Purcell enhancement in plasmonic nanoantennas. *Nat. Photonics* **8**, 835-840 (2014).
21. Pelton, M. Modified spontaneous emission in nanophotonic structures. *Nat. Photonics* **9**, 427–435 (2015).
22. Purcell, E., Torrey, H. & Pound, R. Resonance absorption by nuclear magnetic moments in a solid. Phys. Rev. **69**, 37–38 (1946).
23. Song, J. H. *et al*. Fast and bright spontaneous emission of Er^{3+} ions in metallic nanocavity. *Nat. Commun.* **6**, 7080 (2015).
24. Chikkaraddy, R. *et al*. Single-molecule strong coupling at room temperature in plasmonic nanocavities. *Nature* **535**, 127–130 (2016).
25. Moreau, A. et al. Controlled-reflectance surfaces with film-coupled colloidal nanoantennas. *Nature* **492**, 86–89 (2012).
26. Liang, L. *et al.* Upconversion amplification through dielectric superlensing modulation. *Nat. Commun*. **10**, 1391 (2019).
27. Gargas, D. J. *et al*. Engineering bright sub-10-nm upconverting nanocrystals for single-molecule imaging. *Nat. Nanotechnol.* **9**, 300–305 (2014).
28. Zhang, Q. *et al*. Seed-mediated synthesis of Ag nanocubes with controllable edge lengths in the range of 30-200 nm and comparison of their optical properties. *J. Am. Chem. Soc.* **132**, 11372–11378 (2010).
29. Pollnau, M., Gamelin, D., Lüthi, S., Güdel, H. & Hehlen, M. Power dependence of upconversion luminescence in lanthanide and transition- metal-ion systems. *Phys. Rev. B* **61**, 3337–3346 (2000).
30. Suyver, J., Aebischer, A., García-Revilla, S., Gerner, P. & Güdel, H. Anomalous power dependence of sensitized upconversion luminescence. *Phys. Rev. B* **71**, 125123 (2005).

Acknowledgements

This work is supported by the Singapore Ministry of Education (MOE2017-T2-2-110), Agency for Science, Technology and Research (A*STAR) (Grant NO. A1883c0011), National Research Foundation, Prime Minister's Office, Singapore under its Competitive Research Program (Award No. NRF-CRP15-2015-03) and under the NRF Investigatorship programme (Award No. NRF-NRFI05-2019-0003), and National Natural Science Foundation of China (21771135).

Author contributions

Y.W. and X.L. conceived and designed the experiments. X.L., R.A.L.V, C.Q. and J.K.W.Y supervised the project and led the collaboration efforts. Y.W. and J.X. synthesized the upconversion nanocrystals and silver nanocubes. Y.W., J.X. and E.P. conducted the optical experiments. R.A.L.V, J.X., L.L. and H.L. performed theoretical simulations. Y.W. and X.L. wrote the manuscript with input from all authors. Y.W. and J.X. contributed equally to this work.

Competing financial interests

The authors declare no competing financial interests.

Additional information

Supplementary information is available in the online version of the paper. Reprints and permissions information is available online at http://www.nature.com/reprints. Correspondence and requests for materials should be addressed to X.L. (chmlx@nus.edu.sg) or to R.A.L.V. (renaud.vallee@u-bordeaux.fr).

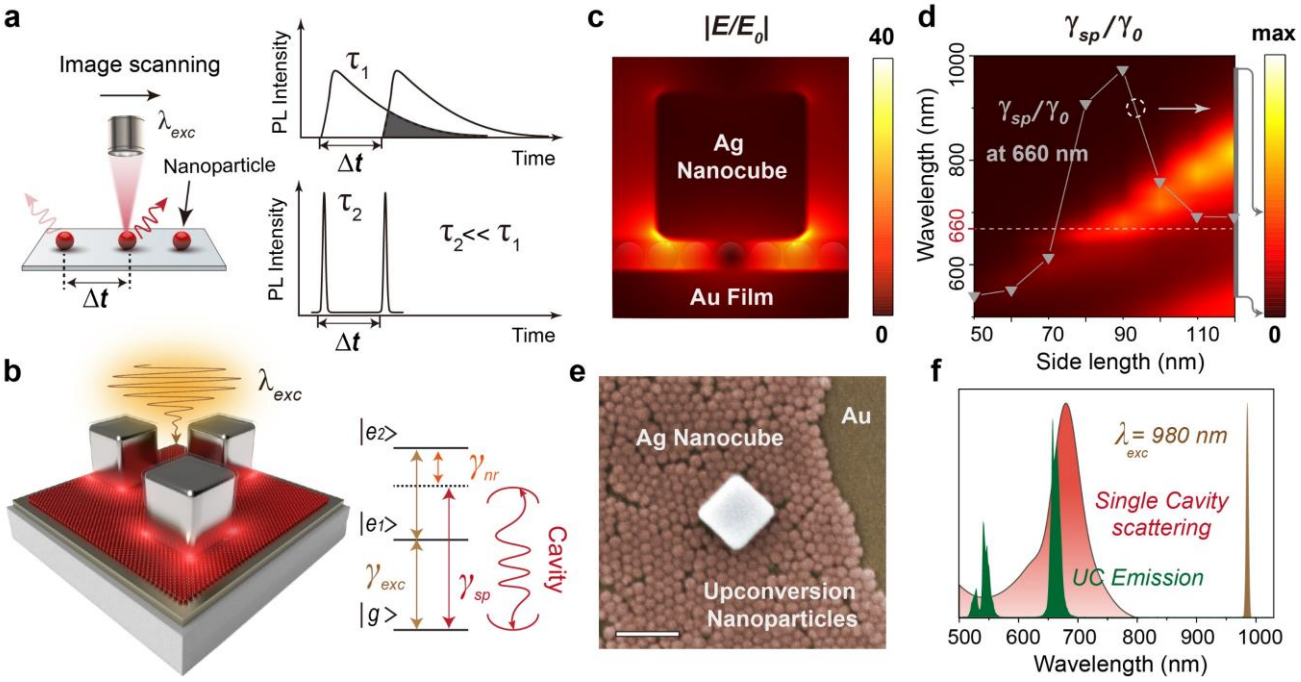

Figure 1 | Upconversion amplification through plasmonic nanocavity coupling. **a,** Schematic representation of the optical signal collection of UCNPs in imaging process over a time interval (Δt). The top-right corner showing that typical UCNPs exhibit long-lived upconversion luminescence (τ_1) under excitation (λ_{exc}). The bottom-right corner showing that the proposed UCNPs with dramatically shortened lifetime (τ_2) permit rapid nonlinear super-resolution imaging. **b,** Rationally designed plasmonic cavity-coupled UCNPs composed of a gold thin film, a silver nanocube, and a monolayer of UCNPs embedded in the sub-20 nm-wide gap (left) and simplified energy-level diagram describing the ESA-mediated upconversion process (right). Note that $|g>$, $|e_1>$ and $|e_2>$ represent the ground state, the first excited state and the second excited state, respectively, while γ_{exc}, γ_{sp} and γ_{nr} denote the excited-state absorption, the radiative decay, and the non-radiative decay process, respectively. The optical cavity is designed to resonantly couple to the emission of UCNPs. **c,** Simulated plasmonic gap mode with a maximum electric field enhancement ($|E/E_0|$) of about 40. **d,** Simulated relative radiative decay rate enhancement at different wavelengths as a function of differently sized silver nanocubes. Grey line shows the optimal condition for decay rate enhancement at a wavelength of 660 nm. **e,** SEM image of a typical plasmonic cavity. Scale bar, 100 nm. **f,** Photoluminescence spectrum of the Er^{3+}-activated UCNPs and simulated scattering spectrum of a single nanocavity. The red upconversion emission spectrum under 980 nm laser excitation overlaps with the plasmonic resonance wavelength at $\lambda \approx 660$ nm.

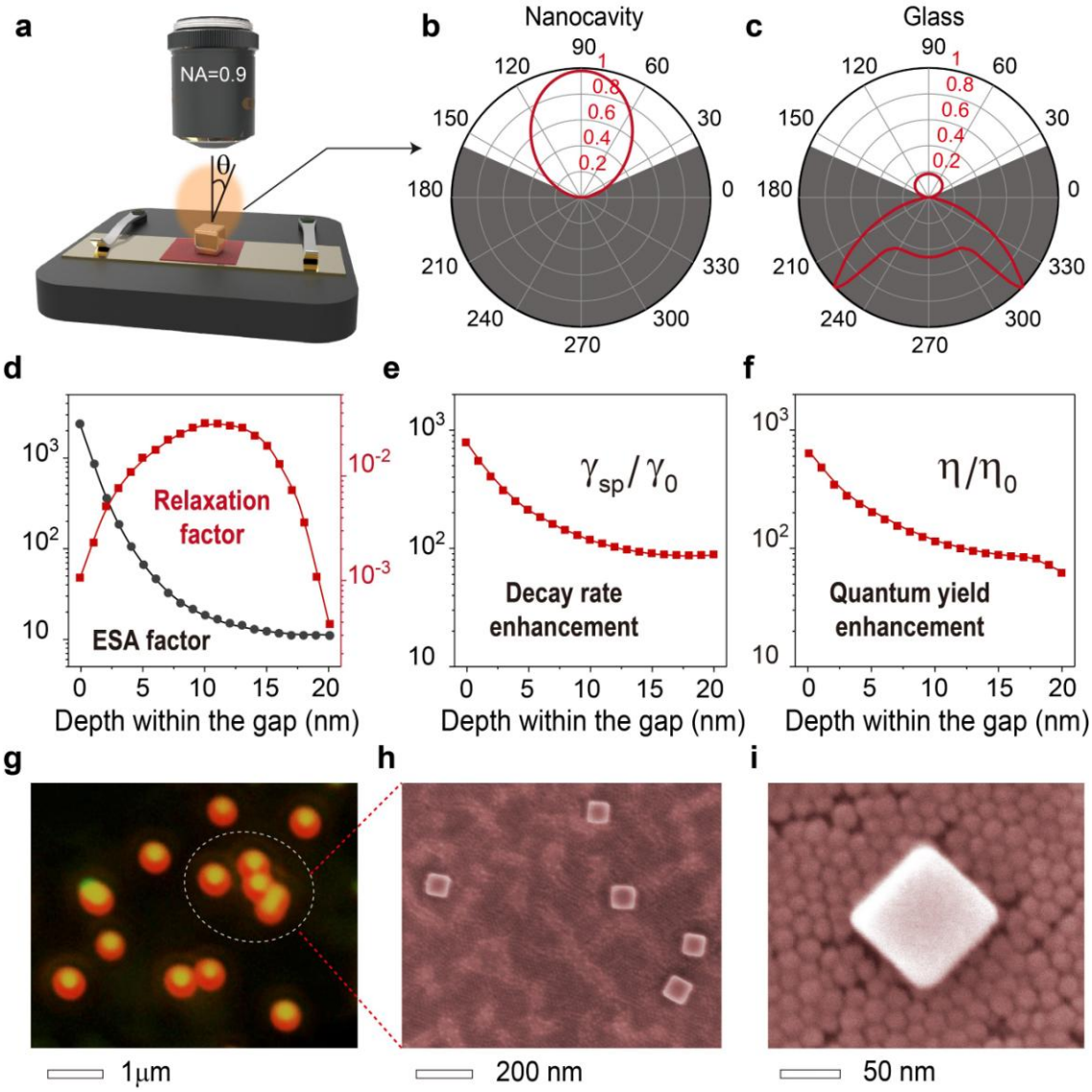

Figure 2 | Theoretical investigations and experimental demonstrations of the gap-plasmon accelerated upconversion process. a, Schematic of the experimental setup designed for luminescence amplification investigation. The brown cone indicates the directionality of the enhanced emission originating from the nanogap region. **b, c,** Far-field angular radiation patterns of UCNPs, simulated by placing the nanoparticles in a single nanoscale cavity and on a glass substrate, respectively. Grey regions represent angular regions, where emission could not be collected due to the limited angular aperture of the used objective. **d,** Local E-field-induced ESA factor (black) and relaxation factor (red), measured as a function of depth within the gap. **e**, **f**, Simulated normalized radiative decay rate and quantum yield enhancement of the emission at 660 nm, measured as a function of depth within the gap. **g,** Photoluminescence imaging of the plasmonic nanocavity effect on upconversion emission, showing the illumination of individual Ag nanocubes by upconversion luminescence. **h,** An enlarged SEM image of the circled region marked in **g** showing the presence of five Ag nanocubes resting on a monolayer of UCNPs. **i,** A high-

resolution SEM characterization showing the placement of a single Ag nanocube on a high-quality monolayer of UCNPs.

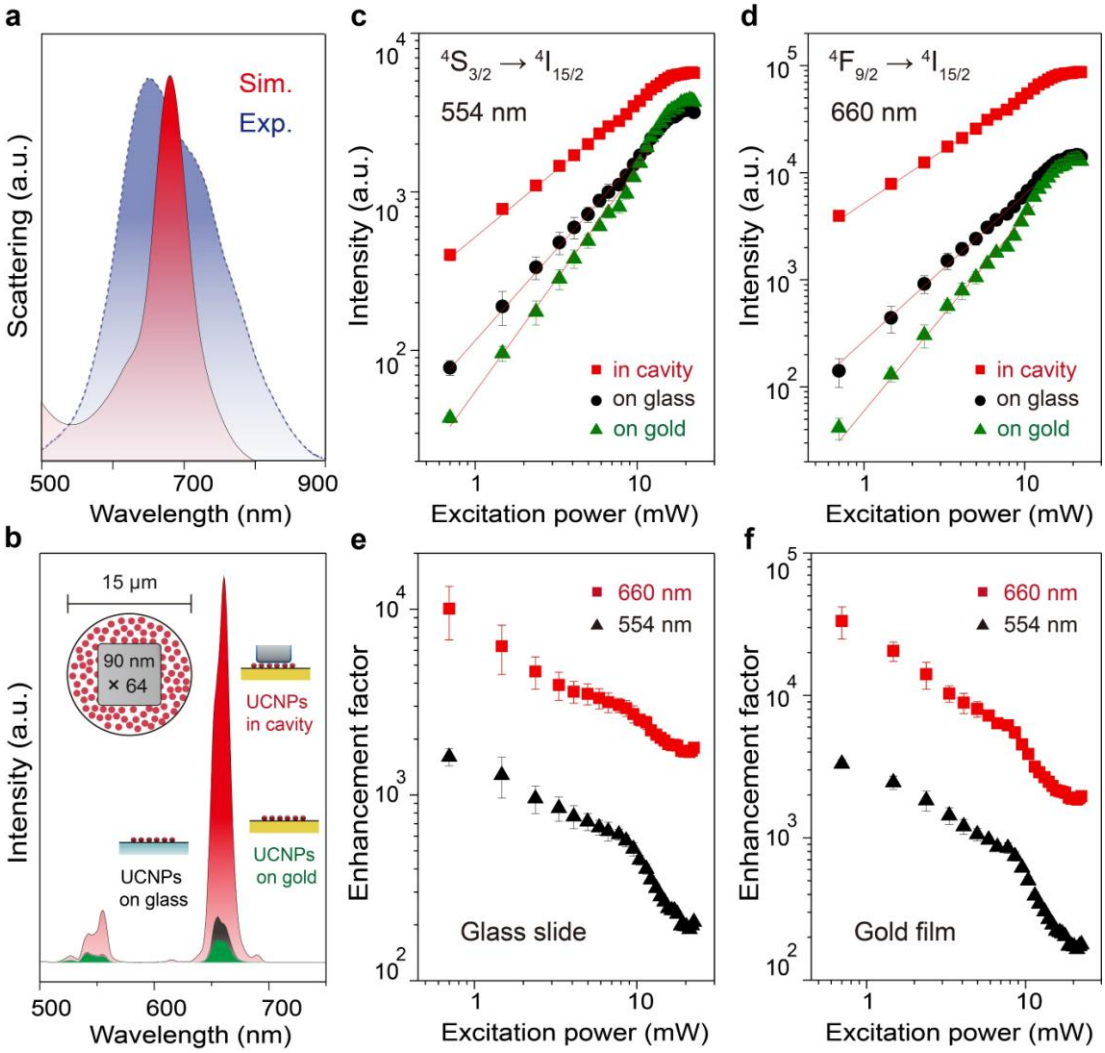

Figure 3 | Spectral properties and luminescence enhancement of UCNPs coupled to a gap-plasmon nanocavity. a, Measured (blue) and simulated (red) scattering spectra of a single nanocavity. **b,** Photoluminescence spectra of an UCNP monolayer deposited on the glass substrate (black) and gold film (green) or in the nanocavity (red). The inset at the top-left showing the schematic of the experimental condition applied for the photoluminescence measurement in the nanocavity mode. **c, d,** The dependence of photoluminescence intensity on the laser excitation power for the three samples at emission wavelengths of 554 nm and 660 nm, respectively. **e, f,** Luminescence enhancement factors as a function of the incident excitation power at emission wavelengths of 554 nm (black) and 660 nm (red), calculated for UCNPs in the nanocavity mode relative to those deposited on the glass substrate and gold film.

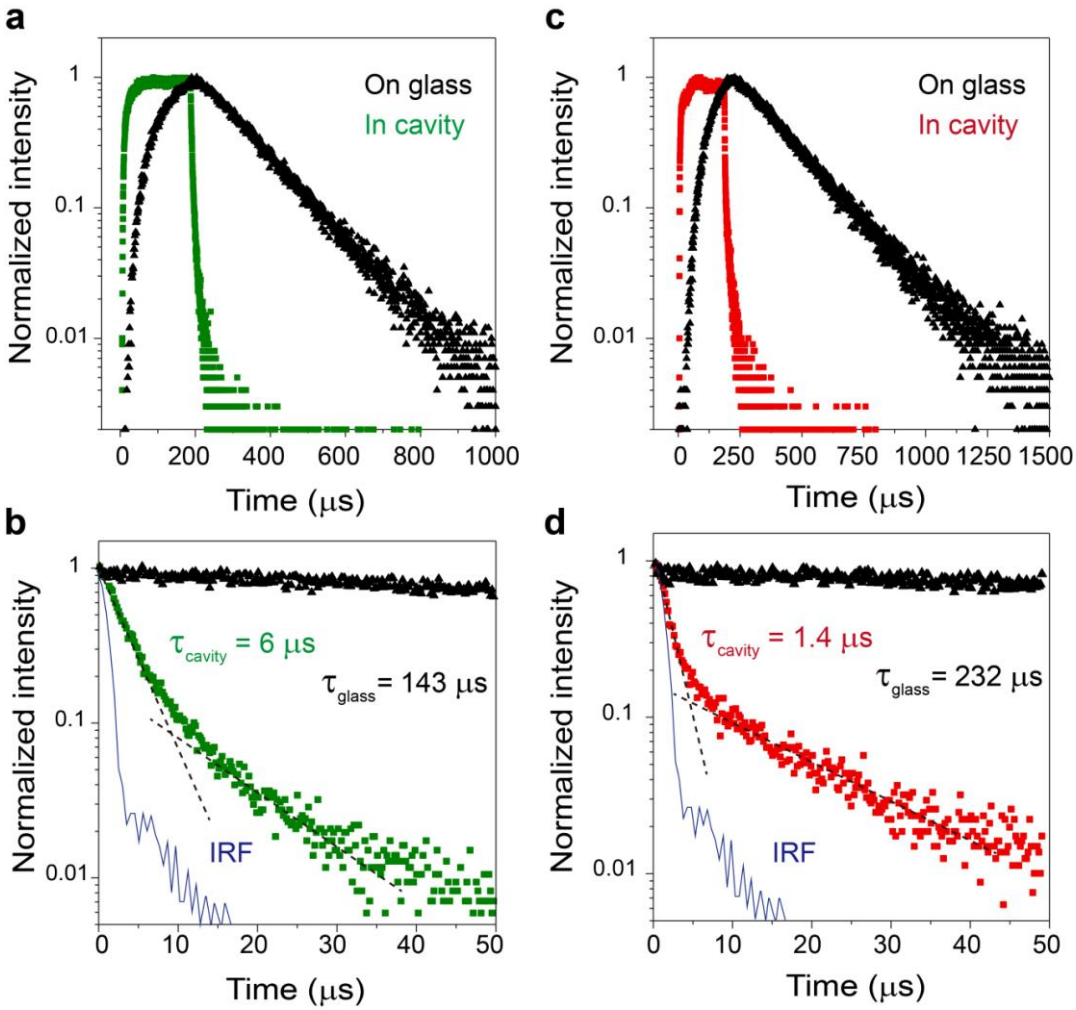

Figure 4 | Spontaneous emission rate measurements of UCNPs. a, Time-resolved photoluminescence measurements of UCNPs deposited on a glass slide (black) and in the nanocavity mode (green) at an emission wavelength of 554 nm. **b,** Comparison of the normalized time-resolved luminescence decay for UCNPs deposited on a glass slide (black) and UCNPs enhanced by the nanocavity mode (green) at an emission wavelength of 554 nm. **c,** Time-resolved photoluminescence measurements of UCNPs deposited on a glass slide (black) and in the nanocavity mode (red) at an emission wavelength of 660 nm. **d,** Comparison of the normalized time-resolved luminescence decay for UCNPs deposited on a glass slide (black) and UCNPs enhanced by the nanocavity mode (red) at an emission wavelength of 660 nm. Note that for **b** and **d**, a single exponential function is used to fit the UCNPs on the glass substrate, while a biexponential function is used to adjust the plasmonic cavity decay. The instrument response function (IRF) is shown in blue.